European Journal of Medicinal Chemistry 216 (2021) 113313

Contents lists available at ScienceDirect

European Journal of Medicinal Chemistry

journal homepage: http://www.elsevier.com/locate/ejmech

Design, synthesis and evaluation of 3-amide-5-aryl benzoic acid derivatives as novel $P2Y_{14}R$ antagonists with potential high efficiency against acute gouty arthritis

Ran Lu [a, b, 1], Yilin Wang [a, 1], Chunxiao Liu [a], Zhenguo Zhang [d], Baiyang Li [a], Zibo Meng [a], Cheng Jiang [a, b, c, *], Qinghua Hu [a, c, **]

[a] School of Pharmacy, China Pharmaceutical University, 639 Longmian Avenue, Nanjing, 211198, PR China
[b] Jiang Su Key Laboratory of Drug Design and Optimization, China Pharmaceutical University, 24 Tongjiaxiang, Nanjing, 210009, PR China
[c] State Key Laboratory of Natural Medicines, China Pharmaceutical University, 24 Tongjiaxiang, Nanjing, 210009, PR China
[d] Institute of Advanced Synthesis, School of Chemistry and Molecular Engineering, Nanjing Tech University, 30 Puzhu South Road, Nanjing, 211816, PR China

ARTICLE INFO

Article history:
Received 25 November 2020
Received in revised form
1 February 2021
Accepted 14 February 2021
Available online 24 February 2021

Keywords:
$P2Y_{14}$ receptor
Antagonist
3-Amide-5-aryl benzoic acid derivatives
Anti-inflammation

ABSTRACT

$P2Y_{14}$ nucleotide receptor plays important roles in series of physiological and pathologic events especially associated with immune and inflammation. Based on the 3-amide benzoic acid scaffold reported by our group previously, a series of 5-aryl-3-amide benzoic acid derivatives were designed as novel $P2Y_{14}$ antagonists with improved pharmacokinetic properties. Among which compound **11m** showed most potent $P2Y_{14}$ antagonizing activity with an IC_{50} value of 2.18 nM, furnishing greatly improved water solubility and bioavailability compared with PPTN. In MSU-induced acute gouty arthritis model in mice, **11m** exerted promising *in vivo* efficacy in alleviating mice paw swelling and inflammatory infiltration. Mechanistically, compound **11m** notably blocked pyroptosis of macrophages through inhibiting NLRP3 inflammasome activation. This work may contribute to the identification of potential therapeutic agents to intervene in acute gouty arthritis.

1. Introduction

P2 purinergic receptors are activated by purine or pyrimidine nucleotides, including inotropic $P2X_{1-7}$ receptors and metabotropic $P2Y_{1,2,4,6,11,12,13,14}$ receptors, which play key roles in physiology and disease [1–4]. $P2Y_{14}$ receptor is a member in P2Y receptors family, which is activated by endogenic UDP-glucose (UDPG) and other UDP sugars [5,6]. $P2Y_{14}$ receptor has been reported broadly expressed in astrocytes, microglia, immune cells and lung epithelial cells [5,7,8].

It has been considered that UDPG coupled $P2Y_{14}$ receptors promoted the hypersensitivity of microglia cells and the fluidity of neutrophils [9–12]. Recent studies showed that knock-out mice suffered a significantly reduced glucose tolerance and changed expression of components involved in insulin secretion, highlighting $P2Y_{14}R$ as a new modulator of maintaining energy homeostasis by influencing insulin release [13,14]. Interestingly, $P2Y_{14}R$ also plays a role in pro-inflammatory cytokines secretion to mediate acute and chronic inflammatory conditions [15,16]. For example, activation of $P2Y_{14}R$ in ischemic acute kidney injury upregulated IRI-induced increase of chemokine expression in collecting duct intercalated cells, and promoted neutrophil and monocyte renal infiltration [17,18]. Another research illustrated that $P2Y_{14}R$ knockout disrupted MSU-induced histopathologic changes in rat synoviums, accompanying with a significant inhibition of pyroptotic cell death and blockade of NRPL3 inflammasome activation in synovial tissues [19].

$P2Y_{14}R$ antagonists have been developed as a potential therapeutic for treating immune and inflammatory diseases. Well-characterized potent and selective $P2Y_{14}R$ antagonists are invaluable tools for testing biological and therapeutic hypotheses. And many efforts have been made to discover antagonists that can be developed into a therapeutic drug (Fig. 1) [20]. The pyrido [4,3-d]

* Corresponding author. School of Pharmacy, China Pharmaceutical University, 639 Longmian Avenue, Nanjing, 211198, PR China.
** Corresponding author. School of Pharmacy, China Pharmaceutical University, 639 Longmian Avenue, Nanjing, 211198, PR China.
E-mail addresses: jc@cpu.edu.cn (C. Jiang), huqh@cpu.edu.cn (Q. Hu).
[1] These authors contributed equally to this study.

https://doi.org/10.1016/j.ejmech.2021.113313
0223-5234/

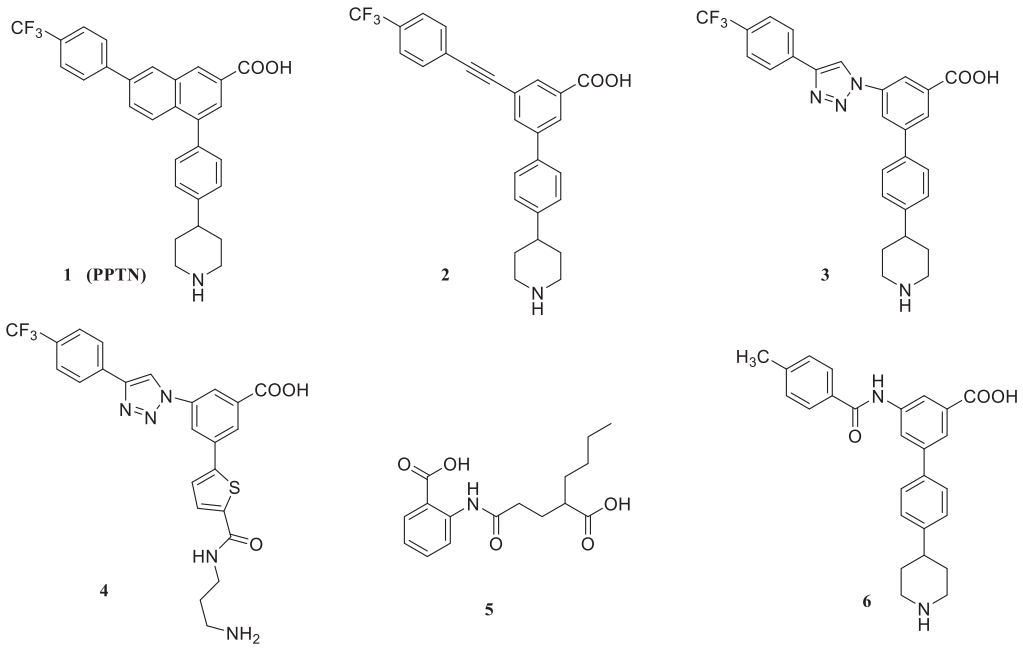

Fig. 1. Representative $P2Y_{14}R$ antagonists.

pyrimidines [21] was the first discovered scaffolds through HTS, accompanying with hERG channel effects. Compound **1** (PPTN), one of the reported 2-naphthalic acids derivatives, was tested for the treatment of renal inflammatory with high activity and high selectivity [22,23]. However, it suffered with poor physicochemical properties and low oral bioavailability [7]. Some strategies have been applied to overcomethis, such as esterifying the carboxyl group into a pro-drug [23], or introduce a strong hydrophilic polyethylene glycol chain on the amino group to increase water solubility [24]. It has been reported several novel structures based on the structure-guided modification and homogenous model [25], including 3-alkynyl (compound **2**) or triazole benzoic acids (compound **3** and **4**) [26,27], 2-amide benzoic acids (compound **5**) [28] and 3-amide benzoic acids (compound **6**) [29]. The 3-amide benzoic acids reported by our group showed potent $P2Y_{14}R$ antagonizing activity and excellent *in vitro* potency. However, the optimized **6** suffered from poor bioavailability (F = 6%) due to its zwitterionic character. In this work, a series of 3-amide-5-aryl benzoic acid derivatives were identified to overcome the limitations through replacing the basic substitutions attached to the core phenyl ring with substituted phenyl or aromatic groups.

2. Results and discussion

2.1. Molecule design

In our previous work, a series of 3-amide benzoic acids were identified as novel and potent $P2Y_{14}R$ antagonists [28]. However, compound **6** showed very poor bioavailability (F = 6%) due to its zwitterionic character. Based on the reported works, the carboxyl group was necessary for maintaining activity, thus the design strategy in this work was to retain the carboxyl group. As it has been reported, the hydrophobic 4-(4-methyl)-benzamide moiety attached to C-3 of the benzoic acid core was considered as the optimal substitution at this position. Additionally, previous SAR exploration of PPTN predicted that a charged amino group is not essential, and diverse 5- and 6-membered ring linking the core facing the extracellular loop side of the receptor were also efficient. Therefore, we introduced phenyl or heterocyclic group to replace the phenylpiperidine in order to find new $P2Y_{14}R$ antagonists with improved pharmacokinetic properties. A series of new 3-amide-5-aryl benzoic acids were designed as shown in Table 1.

2.2. Chemistry

The synthetic route of target compounds was outlined in Scheme 1. The commercially available 3-amino-5-bromobenzoic acid (**7**) was methylated with $SOCl_2$ in menthol to produce methyl 3-amino-5-bromobenzoate (**8**). Subsequent coupling of the obtained bromobenzoate ester with 4-methylbenzoic acid using BOP reagent in the presence of DMAP as a base gave key intermediate (**9**). Then the resulted bromobenzoate esters were coupled with appropriate aromatic boric acids or borates catalyzed with Pd $(PPh_3)_4$ and Cs_2CO_3 in DMF under argon conditions to provide the expected analogues of this series. Finally, the target compounds, 3-(4-methylbenzamido) benzoic acids derivatives (**11a-11q**), were obtained by hydrolyzing the corresponding methyl 3-bromo-5-(4-methylbenzamido) benzoates in an aqueous solution of lithium hydroxide with yield ranging from 74% to 89%.

2.3. Biological evaluation

2.3.1. In vitro $P2Y_{14}R$ inhibition

All synthesized derivatives were tested for their *in vitro* inhibition based on the production of cAMP in a HEK293 cell line stably expressing $P2Y_{14}R$. The $P2Y_{14}R$ inhibitory activities of these derivatives were screened at a relatively high single concentration of inhibitor (100 nM) to identify the more potent antagonist. The IC_{50} values of the compounds with more than 80% inhibition at 100 nM were further tested in the functional assay with full concentration-response curves as shown in Table 1.

Firstly, piperidine group in **6** was removed and **11a** was obtained. This modification did not lose potency dramatically (IC_{50} = 4.85 nM). When phenyl was substituted with electron-donating group (4-CH_3O-), the $P2Y_{14}R$ inhibitory activities was slightly decreased. Furthermore, the water solubility of **11a** was

Table 1
In vitro $P2Y_{14}R$ affinity and cLogP values of compounds **11a-q**.

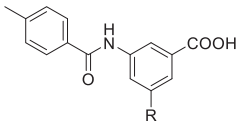

Compound	R	$P2Y_{14}R$ affinity		cLog P
		% inhibition at 100 nM	IC_{50} (nM)	
PPTN (**2**)	–	96.31	1.98 ± 0.006	6.18
6	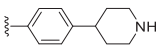	85.33	1.77 ± 0.26	4.05
11a		86.99	4.85 ± 1.49	4.56
11b	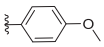	79.10	ND	4.43
11c		79.10	ND	3.22
11d		72.12	ND	3.22
11e		65.72	ND	2.62
11f	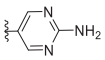	68.57	ND	2.33
11g	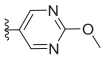	72.50	ND	3.01
11h		82.96	9.74 ± 0.19	4.48
11i		68.76	ND	4.54
11j		60.19	ND	4.88
11k		43.70	ND	3.91
11l		61.09	ND	3.17
11m		93.39	2.18 ± 0.42	3.12
11n		16.05	ND	3.51
11o		82.27	2.95 ± 0.47	3.77
11p		46.01	ND	3.1
11q		86.79	2.63 ± 0.67	3.08

decreased compared with **6**. Next several five or six-membered heterocyclic rings as the bioisostere of phenyl ring were introduced to replace the phenyl group in order to improve the aqueous solubility. According to the results of $P2Y_{14}R$ affinities, compounds (**11c**, **11d** and **11e**) replaced by nitrogen-containing aromatic heterocycles didn't exhibit a good inhibition ratio (<80%). Compounds that displayed inhibition of >80% on the $P2Y_{14}$ R at 100 nM were five-membered heterocyclic rings containing one heteroatom at position 3 of these structure, such as S (**11h**, 82.96%), O (**11m**, 93.39%; **11o**, 82.27%), NH (**11q**, 86.79%). A closer inspection of the affinity data reveals that, in most cases, the introduction of pentagonal heterocycles linked at position 2 (compound **11k-m**, **11o-p** and **11r**), diminishes the affinity compared to the 3-substituted ones. For example, the 3-furyl derivative **11m** was considered as the most appealing $P2Y_{14}R$ antagonist (93.39% inhibition at 100 nM, IC_{50} = 2.18 nM) identified in this work, while its close analogue **11l** exhibited a decreased $P2Y_{14}R$ inhibitory activity (61.09% inhibition at 100 nM). Moreover, other compounds for instance a thienyl or furyl group substituted by a methyl (**11j**, **11n**) or acetyl (**11k**) at position 3 showed decreased affinity. The IC_{50}

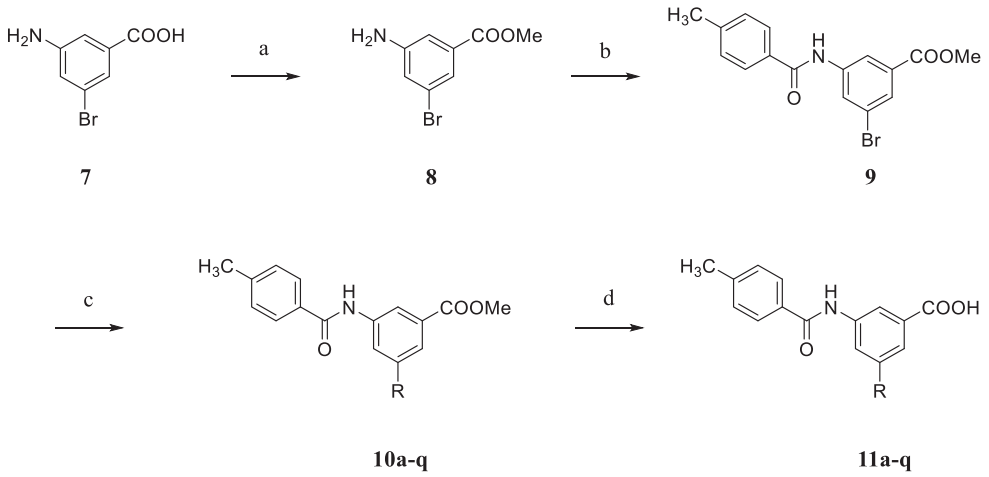

Scheme 1. Reagents and conditions:(a) CH_3OH, $SOCl_2$, 0–25 °C; (b) BOP reagent, DMAP, DCM; (c) $Pd(PPh_3)_4$, Cs_2CO_3, DMF, 100 °C; (d) LiOH(1 M aq). MeOH- THF-DMSO 1/1/1 (v/v/v). **R** are defined in Table 1.

values of the compounds with more than 80% inhibition to the $P2Y_{14}$ R at 100 nM were further tested in the functional assay with full concentration-response curves as shown in Table 1. The IC_{50} values for **11a**, **11h**, **11m**, **11o** and **11q** were 4.85, 9.74, 2.18, 2.95 and 2.63 nM, respectively.

After optimization, several highly potent $P2Y_{14}$R antagonists were obtained. Compounds **11o** and **11q**, two of the most potent compounds, were chemically unstable, which were oxidized easily at room temperature in DMSO. Thus, the stable and most potent one, **11m**, was selected for further evaluation.

2.3.2. Metabolic stability of *11m* in human liver microsomes

11m was evaluated for its metabolic stability in human microsomes. Compound **11m** demonstrated excellent microsomal stability ($T_{1/2}$ > 60 min).

2.3.3. Pharmacokinetic (PK) study of compound *11m* in SD mice

Compound **11m** was evaluated for pharmacokinetics (PK) in male SD mice at 5 mg/kg and 10 mg/kg for intravenous (iv) and oral (po) administration. As shown in Table 2, **11m** showed dramatically improved oral bioavailability (48.32% for compound **11m** *vs* 7% for compound **PPTN**) and more favorable PK profile. The moderate volume of distribution (Vss) of 0.78 L/kg suggested that compound **11m** penetrated to tissues well, and high systemic exposure (oral AUC_{all} = 436599 min*ng/mL) indicated that compound **11m** could be well absorbed after oral administration, while the oral AUC_{all} value of compound **1** was 182083 min*ng/mL. Compound **11m** exhibited reasonable plasma clearance level (CL = 6.03 mL/min/kg) and half-life ($T_{1/2}$ = 138.93 min and 153.54 min for iv and oral administration, respectively). According to the results, bioavailability of **11m** was greatly improved compared with PPTN (F = 7%) or compound **6** (F = 6%).

2.3.4. Water solubility

An important aim in the development of new $P2Y_{14}$R antagonists is to improve the aqueous solubility. PPTN has an aqueous solubility less than 0.005 mg/mL, and the solubility of **11a** is 0.0463 mg/mL (pure water). While **11m** shows an aqueous solubility of 0.0776 mg/mL (pure water), which is more than 10-fold improvement compared with PPTN and more than 1.5-fold for **11a**.The improved aqueous solubility will provide an opportunity to evaluate their *in vivo* functional profiles.

2.3.5. Anti-inflammatory effects of compound *11m*

As shown in Fig. 2, in MSU-induced animal model, control mice with MSU treatment showed a continuous stability of paw

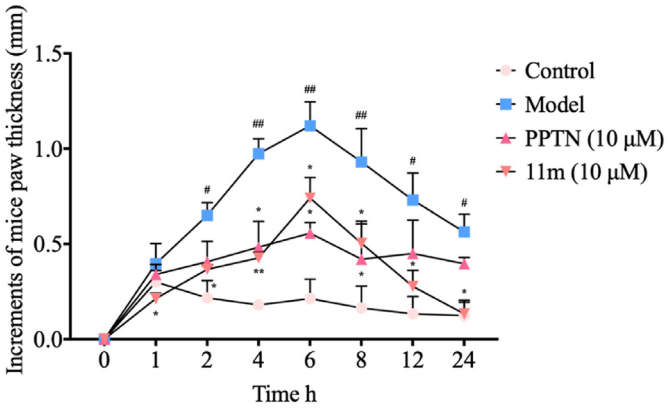

Fig. 2. The thickness of mice foot was increased after the injection of MSU. PPTN and **11m** abolished the effective effect on the paw swelling. The injected foot thickness of each mouse was determined at 0, 1, 2, 4, 6, 8, 12, 24 h after MSU stimulation (n = 6). Data are shown as means ± SD (n = 3). $^{\#}P < 0.05$, $^{\#\#}P < 0.01$ versus control group, $^{*}P < 0.05$, $^{**}P < 0.01$ versus model group.

Table 2
Pharmacokinetic (PK) results of compound **11m**.

compounds	admin (dosage)	sample	C_{max} (ng/mL)	$T_{1/2}$(min)	AUC_{all} (min*ng/mL)	V_{ss} (mL/kg)	CL (mL/min/kg)	F(%)
11m	iv (5 mg/kg)[a]	plasma	19270[b]	138.93	843849	781.93	121.95	
	po (10 mg/kg)[a]	plasma	1801	153.54	436599.5	212.67	6.03	48.32%

[a] n = 5.
[b] Cmax = C_5 (t = 5 min) for iv administration.

thickness during experimental period. In contrast, an obvious elevation in paw thickness could be observed in model mice receiving MSU, suggesting the occurrence of exaggerated paw swelling. Most importantly, **11m** or PPTN treatment efficiently reversed the paw swelling and infiltration of inflammatory cells in foot tissues (Fig. 3). Besides, compound **11m** was similar to PPTN in the first 4 h, however, it recovered paw swelling more significantly after 24 h.

MSU stimulation contribute to the up-regulation of NLRP3, ASC and Caspase-1 p20 protein expressions in mice foot tissues compared with control group, which were reversed by treatment of compound **11m** and PPTN. Meanwhile, increased level of IL-1β, IL-8 and GSDMD-NT in model group were apparently inhibited by compound **11m** and PPTN (Fig. 4).

Consistently, MSU exposure in the model group exhibited an obvious increment in the proportion of pyroptotic cells characterized by Caspase-1/PI double positive staining analyzed by flow cytometry compared with control ones (Fig. 5), which was notably ameliorated by **11m** and PPTN intervention.

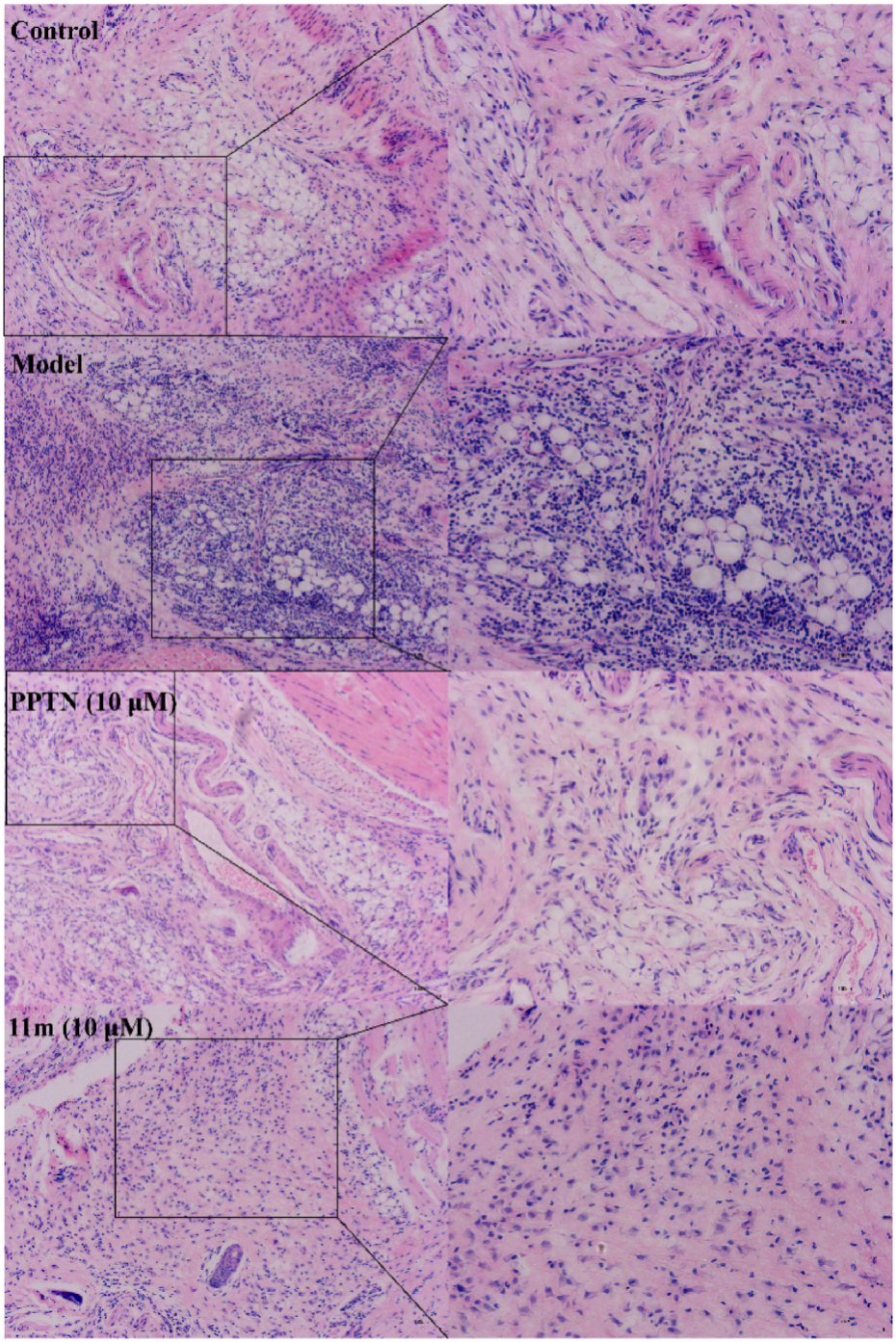

Fig. 3. Representative photographs of histo-pathological changes in foot tissues are presented (200 × , 400 ×). The small boxed areas show higher magnification views of the large boxes.

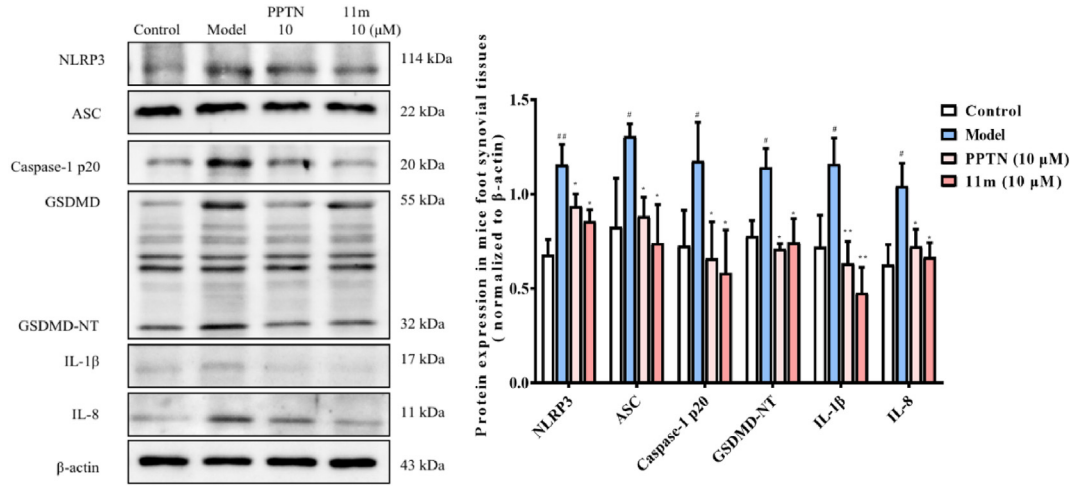

Fig. 4. (A) Relative protein expressions of NLRP3, ACS, Caspase-1 (p20), GSDMD, IL-1β and IL-8 in foot tissues were assayed by western blot. (B) Quantification of the protein level was expressed as the ratio (in percentage) of control group. Data are shown as means ± SD (n = 3). $^{###}P < 0.001$ versus control group, $^{*}P < 0.05$, $^{**}P < 0.01$ versus model group.

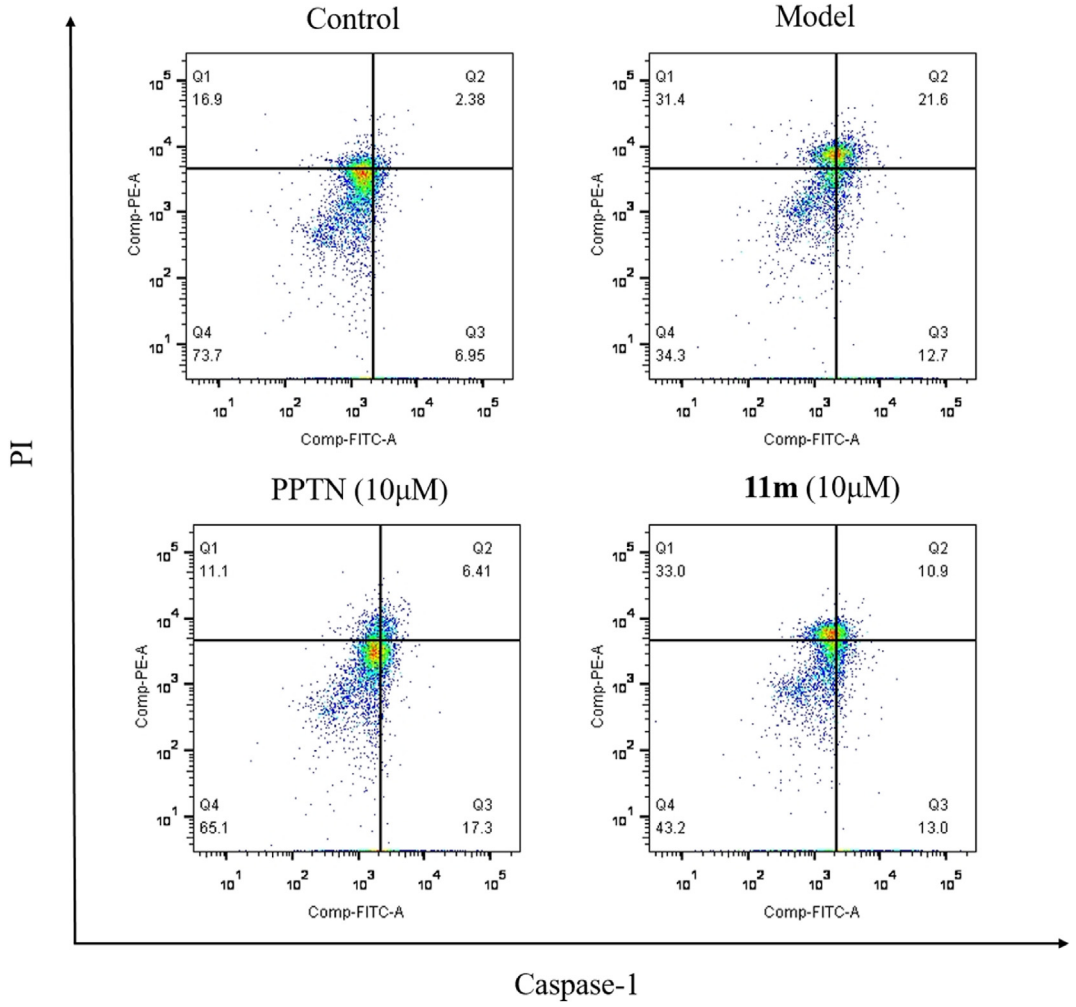

Fig. 5. Effects of compound **11m** and PPTN on MSU-induced pyroptosis of macrophages in mice air pouch exudates. The rate of pyroptotic cell death was examined with PI and active Caspase-1 double staining by flow cytometry.

3. Conclusion

In summary, a series of 3-amide-5-aryl benzoic acids were identified as novel $P2Y_{14}R$ antagonists with improved pharmacokinetic profiles by zwitterionic character. The optimized compound **11m** showed potent $P2Y_{14}R$ antagonizing activity and the water

solubility of **11m** was greatly improved compared with PPTN. Compound **11m** showed excellent microsomal stability in human microsomes and moderate bioavailability (F = 48%) in rats. *In vivo* anti-inflammatory evaluation of **11m** in MSU-induced mice paw swelling model demonstrated that **11m** can efficiently reversed the paw swelling and infiltration of inflammatory cells in foot tissues. Most importantly, in the MSU-induced mice paw swelling model, **11m** exerted better therapeutic effects in lowering increments of mice paw thickness (~0.13 mm) than PPTN (~0.40 mm) at 24 h, exhibiting more potential $P2Y_{14}R$ inhibitory actions. On the other hand, **11m** significantly reversed NLRP3 inflammasome activation induced by MSU-injection, contributing to decreased proportion of pyroptosis macrophages. Taken together, the identification of the 3-amide-5-aryl benzoic acids $P2Y_{14}$ receptor antagonists with preferred *in vitro* and *in vivo* potencies may provide an alternative therapy for acute gouty arthritis diseases.

4. Experimental

4.1. Chemistry

All reagents and solvents were commercially available and were used without further purification. The high-resolution mass spectroscopic (HRMS) data were obtained on a proteomics optimized Q-TOF-2 (Micromass-Waters) using external calibration with polyalanine. ^{1}H NMR and ^{13}C NMR spectra were recorded on Bruker 400 MHz or Bruker 300 MHz instruments using the solvent indicated in each case (300 MHz or 400 MHz for ^{1}H and 75 or 101 MHz for ^{13}C). The tested compounds were purified to >95% purity as determined by HPLC. All chemical reagents were purchased from bide. All reactions were monitored by thin-layer chromatography (TLC) with 254 nm and 365 nm fluorescent indicators. The purification of compounds by flash chromatography and preparative TLC was carried out using silica-gel 300*400 mm mesh and GF254 plates, respectively. C LogP was calculated using ALOGPS 2.1 program (www.vcclab.org/lab/alogps/). PPTN (**1**) was prepared as the reported [22]. Compound **5** were synthesized according to our previous work [28].

4.1.1. Synthesis of methyl 3-amino-5-bromobenzoate (*8*)

To a solution of 3-amino-5-bromobenzoic acid (**7**) (5.00g, 23.14 mmol) in methanol (25 mL) was added $SOCl_2$ (15 mL) dropwise at 0 °C. Then, the mixture was stirred at room temperature for 2 h and was monitored by TLC. After the reaction completed, the reaction was added saturate sodium hydrogen carbonate aqueous solution until pH 7–8, followed stirring for another 30 min. The mixture was extracted with ethyl acetate (50 mL* 3). The organic phase was collected and dried over $MgSO_4$. After filtration, the solvent was removed under reduced pressure and the residue was purified by column chromatography (petroleum ether/ethyl acetate = 1:1) to provide the pure product as white solid. Yield: 4.62g, 86.4%. m. p. 94–95 °C. ^{1}H NMR (300 MHz, $CDCl_3$-d_3) *(ppm)* 7.55 (t, J = 1.6 Hz, 1H), 7.28 (dd, J = 2.4, 1.4 Hz, 1H), 7.01 (t, J = 2.0 Hz, 1H), 3.91 (s, 3H). MS (ESI-TOF) *m/z* calc'd for $C_{18}H_{15}N_3O_3$ $[M+H]^+$ 229.9817, found 229.9814.

4.1.2. Synthesis of methyl 3-bromo-5-(4-methylbenzamido) benzoate (*9*)

To a magnetically stirred suspension of 4-methylbenzoic acid (4.44g, 32.60 mmol) in DCM (35 mL) were successively added N, N-dimethylpyridin-4-amine (DMAP) (5.31g, 43.46 mmol) and BOP reagent (14.42g, 32.60 mmol). The mixture was allowed to stir at room temperature for 15 min. The methyl 3-amino-5-bromobenzoate (8) (5.00g, 21.73 mmol) was then added, and the solution was stirred at room temperature overnight. The mixture was washed with 1M hydrochloric acid (20 mL*3). The organic layer were dried over $MgSO_4$ and the solvent was eliminated under reduced pressure to give crude product. The residue was purified by column chromatography (petroleum ether/ethyl acetate = 4:1) to give pure **9** as a white solid. Yield: 6.38g, 84%. m. p. 146–147 °C. ^{1}H NMR (400 MHz, $CDCl_3$-d_3) δ *(ppm)* 8.34 (t, J = 2.0 Hz, 1H), 8.07 (t, J = 1.7 Hz, 1H), 7.93 (t, J = 1.6 Hz, 1H), 7.79 (d, J = 8.2 Hz, 2H), 7.30 (d, J = 9.1 Hz, 2H), 3.92 (s, 3H), 2.44 (s, 3H). MS (ESI-TOF) *m/z* calc'd for $C_{18}H_{15}N_3O_3$ $[M+H]^+$ 348.0234, found 426.1857.

4.1.3. General procedure for the synthesis of *11a*-*11q*

(1) To a solution of methyl 3-bromo-5-(4-methylbenzamido) benzoate (200 mg, 0.57 mmol) in DMF (3 mL) was added phenylboronic acid (84 mg, 0.69 mmol), cesium carbonate (281 mg, 0.86 mmol) and $Pd(PPh_3)_4$ (66 mg, 0.057 mmol). The mixture was stirred under argon for 10 h at 100 °C. Upon completion, the mixture was filtered, diluted with ethyl acetate (10 mL * 3), washed with brine, dried over anhydrous $MgSO_4$ and concentrated to give a crude resin. The crude product was further purified using column chromatography (petroleum ether/ethyl acetate = 1:1) to give a white solid of **10a.**

(2) A mixture of methyl 5-(4-methylbenzamido)-[1,1′-biphenyl]-3-carboxylate (1 mmol) (**10a**), 1M LiOH aqueous (5 mL), MeOH (2 mL), DMSO (2 mL) and THF (2 mL) was stirred at room temperature for 3 h. The solvent was concentrated in a vacuum, and the residue was acidified with 1M hydrochloric acid to pH 1. The resulting precipitate was filtered giving rise to corresponding 5-(4-methylbenzamido)-[1,1′-biphenyl]-3-carboxylic acid (**11a**). Purified by preparative TLC (ethyl acetate: methanol = 10:1).

*4.1.3.1. 5-(4-Methylbenzamido)-[1,1′-biphenyl]-3- carboxylic acid (**11a**).* A white solid, yield: 87%; HPLC purity: 96.95%. m. p. 260 °C (decomposed). ^{1}H NMR (400 MHz, DMSO-d_6) δ *(ppm)* 13.10 (s, 1H), 10.42 (s, 1H), 8.46 (t, J = 1.8 Hz, 1H), 8.38 (t, J = 2.0 Hz, 1H), 8.00–7.87 (m, 3H), 7.72–7.68 (m, 1H), 7.68 (s, 1H), 7.53 (dd, J = 8.4, 6.9 Hz, 2H), 7.46–7.40 (m, 1H), 7.38 (s, 1H), 7.36 (s, 1H), 2.40 (s, 3H). ^{13}C NMR (75 MHz, DMSO-d_6) δ *(ppm)* 167.70, 166.06, 142.31, 141.38, 140.65, 139.89, 132.44, 132.15, 129.58, 129.41, 128.43, 128.22, 127.19, 123.04, 122.94, 120.51, 21.46.MS (ESI-TOF) *m/z* calc'd for $C_{21}H_{17}NO_3$ $[M+H]^+$ 332.1287, found 332.1281.

*4.1.3.2. 4′-Methoxy-5-(4-methylbenzamido)-[1,1′-biphenyl]-3-carboxylic acid (**11b**).* A white solid, yield: 87%; HPLC purity: 99.78%. m. p. 247 °C (decomposed). ^{1}H NMR (300 MHz, DMSO-d_6) δ *(ppm)* 13.05 (s, 1H), 10.41 (s, 1H), 8.43 (t, J = 1.7 Hz, 1H), 8.34 (t, J = 1.9 Hz, 1H), 7.95 (d, J = 8.2 Hz, 2H), 7.89 (t, J = 1.6 Hz, 1H), 7.63 (d, J = 8.8 Hz, 2H), 7.36 (d, J = 7.8 Hz, 2H), 7.08 (d, J = 8.8 Hz, 2H), 3.81 (s, 3H), 2.39 (s, 3H). ^{13}C NMR (75 MHz, DMSO-d_6) δ *(ppm)* 167.70, 165.99, 159.74, 142.31, 140.99, 140.55, 132.28, 132.16, 132.11, 129.43, 128.29, 128.21, 122.51, 122.40, 119.82, 115.01, 55.66, 21.49. MS (ESI-TOF) *m/z* calc'd for $C_{22}H_{19}NO_4$ $[M+H]^+$ 362.1392, found 362.1390.

*4.1.3.3. 3-(4-Methylbenzamido)-5-(pyridin-3-yl)benzoic acid (**11c**).* A white solid, yield: 75%; HPLC purity: 99.82%. m. p. 290 °C (decomposed). ^{1}H NMR (400 MHz, DMSO-d_6) δ *(ppm)* 13.19 (s, 1H), 10.48 (s, 1H), 8.94–8.86 (m, 1H), 8.64 (d, J = 4.7 Hz, 1H), 8.53 (s, 1H), 8.41 (d, J = 2.0 Hz, 1H), 8.11 (dt, J = 8.1, 1.9 Hz, 1H), 7.94 (d, J = 8.1 Hz, 3H), 7.55 (dd, J = 8.0, 4.8 Hz, 1H), 7.37 (d, J = 7.8 Hz, 2H), 2.40 (s, 3H). ^{13}C NMR (101 MHz, DMSO-d_6) δ *(ppm)* 167.45, 166.06, 149.50, 148.04, 142.43, 140.77, 138.33, 135.43, 134.81, 132.65, 132.03, 129.47, 128.22, 124.54, 123.10, 123.07, 121.05, 21.51. MS (ESI-TOF) *m/z* calc'd

for $C_{20}H_{16}N_2O_3$ $[M+H]^+$ 333.1239, found 333.1238.

*4.1.3.4. 3-(4-Methylbenzamido)-5-(pyridin-4-yl)benzoic acid (**11d**).* A white solid, yield: 81%; HPLC purity: 99.04%. m. p. 215–217 °C.^{1}H NMR (300 MHz, DMSO-d_6) *δ (ppm)* 13.52 (s, 1H), 10.50 (s, 1H), 8.70 (d, J = 5.0 Hz, 2H), 8.55 (t, J = 2.0 Hz, 1H), 8.49 (t, J = 2.0 Hz, 1H), 8.02 (t, J = 1.7 Hz, 1H), 7.95 (d, J = 7.9 Hz, 2H), 7.72 (d, J = 5.7 Hz, 2H), 7.38 (d, J = 7.9 Hz, 2H), 2.41 (s, 3H). ^{13}C NMR (101 MHz, DMSO-d_6) *δ (ppm)* 167.34, 166.10, 150.90, 146.80, 142.48, 140.87, 138.50, 132.73, 131.98, 129.48, 128.22, 122.95, 122.92, 121.99, 121.79, 21.51. MS (ESI-TOF) *m/z* calc'd for $C_{20}H_{16}N_2O_3$ $[M+H]^+$ 333.1239, found 333.1238.

*4.1.3.5. 3-(4-Methylbenzamido)-5-(pyrimidin-5-yl)benzoic acid (**11e**).* A white solid, yield:84%; HPLC purity: 95.79%. m. p. 151–154 °C.^{1}H NMR (300 MHz, DMSO-d_6) *δ (ppm)* 13.20 (s, 1H), 10.50 (s, 1H), 9.25 (s, 1H), 9.14 (s, 2H), 8.55 (t, J = 1.8 Hz, 1H), 8.41 (t, J = 1.9 Hz, 1H), 8.01 (t, J = 1.6 Hz, 1H), 7.94 (d, J = 8.2 Hz, 2H), 7.36 (d, J = 8.3 Hz, 2H), 2.40 (s, 3H). ^{13}C NMR (75 MHz, DMSO-d_6) *δ (ppm)* 167.31, 166.06, 158.15, 155.32, 142.47, 140.87, 135.11, 133.30, 132.88, 131.94, 129.47, 128.22, 123.20, 123.14, 121.72, 21.50. MS (ESI-TOF) *m/z* calc'd for $C_{19}H_{15}N_3O_3$ $[M+H]^+$ 334.1192, found 334.1190.

*4.1.3.6. 3-(2-Aminopyrimidin-5-yl)-5-(4-methylbenzamido)benzoic acid (**11f**).* A white solid, yield: 89%; HPLC purity: 99.40%. m. p. 242–244 °C. ^{1}H NMR (300 MHz, DMSO-d_6) *δ (ppm)* 13.11 (s, 1H), 10.40 (s, 1H), 8.58 (s, 2H), 8.43 (t, J = 1.7 Hz, 1H), 8.24 (t, J = 1.9 Hz, 1H), 7.93 (d, J = 8.2 Hz, 2H), 7.85 (t, J = 1.6 Hz, 1H), 7.37 (d, J = 8.0 Hz, 2H), 6.91 (s, 2H), 2.40 (s, 3H). ^{13}C NMR (75 MHz, DMSO-d_6) *δ (ppm)* 167.58, 165.98, 163.61, 156.46, 142.38, 140.64, 136.50, 132.52, 132.08, 129.46, 128.20, 121.86, 121.54, 119.99, 21.51. MS (ESI-TOF) *m/z* calc'd for $C_{19}H_{16}N_4O_3$ $[M+H]^+$ 349.1301, found 349.1290.

*4.1.3.7. 3-(2-Methoxypyrimidin-5-yl)-5-(4-methylbenzamido)benzoic acid (**11g**).* A white solid, yield: 86%; HPLC purity: 99.62%. m. p. 166–168 °C. ^{1}H NMR (300 MHz, DMSO-d_6) *δ (ppm)* 10.47 (s, 1H), 8.93 (s, 2H), 8.50 (t, J = 1.7 Hz, 1H), 8.32 (t, J = 1.9 Hz, 1H), 7.99–7.88 (m, 3H), 7.37 (d, J = 8.0 Hz, 2H), 3.99 (s, 3H), 2.40 (s, 3H). ^{13}C NMR (101 MHz, DMSO-d_6) *δ (ppm)* 168.28, 166.91, 166.11, 158.73, 143.28, 141.60, 136.02, 133.54, 132.86, 130.31, 129.07, 128.29, 128.20, 123.48, 121.91, 56.15, 22.35. MS (ESI-TOF) *m/z* calc'd for $C_{20}H_{17}N_3O_4$ $[M+H]^+$ 364.1297, found 364.1293.

*4.1.3.8. 3-(4-Methylbenzamido)-5-(thiophen-3-yl)benzoic acid (**11h**).* A white solid, yield: 83%; HPLC purity: 99.42%. m. p. 258 °C (decomposed). ^{1}H NMR (300 MHz, DMSO-d_6) *δ (ppm)* 13.10 (s, 1H), 10.38 (s, 1H), 8.45–8.33 (m, 2H), 7.95 (d, J = 2.9 Hz, 2H), 7.93–7.88 (m, 2H), 7.70 (dd, J = 5.2, 2.8 Hz, 1H), 7.52 (d, J = 5.0 Hz, 1H), 7.36 (d, J = 7.9 Hz, 2H), 2.40 (s, 3H). ^{13}C NMR (75 MHz, DMSO-d_6) *δ (ppm)* 167.79, 166.04, 142.30, 141.11, 140.54, 136.26, 132.59, 132.15, 129.41, 128.22, 127.99, 126.46, 122.45, 122.38, 122.28, 120.38, 21.46. MS (ESI-TOF) *m/z* calc'd for $C_{19}H_{15}NO_3S$ $[M+H]^+$ 338.0851, found 338.0852.

*4.1.3.9. 3-(4-Methylbenzamido)-5-(thiophen-2-yl)benzoic acid (**11i**).* A white solid, yield: 88%; HPLC purity: 96.35%. m. p. 260 °C (decomposed). ^{1}H NMR (300 MHz, DMSO-d_6) *δ (ppm)* 13.22 (s, 1H), 10.41 (s, 1H), 8.39 (d, J = 3.1 Hz, 2H), 7.95 (s, 1H), 7.92 (d, J = 2.3 Hz, 2H), 7.69–7.46 (m, 2H), 7.36 (d, J = 7.9 Hz, 2H), 7.18 (dt, J = 6.3, 3.1 Hz, 1H), 2.40 (s, 3H). ^{13}C NMR (75 MHz, DMSO-d_6) *δ (ppm)* 167.39, 166.08, 142.82, 142.40, 140.76, 134.79, 132.54, 132.05, 129.44, 129.19, 128.23, 126.88, 124.76, 121.33, 121.26, 120.41, 21.51. MS (ESI-TOF) *m/z* calc'd for $C_{19}H_{15}NO_3S$ $[M+H]^+$ 338.0851, found 338.0851.

*4.1.3.10. 3-(4-Methylbenzamido)-5-(5-methylthiophen-2-yl)benzoic acid (**11j**).* A white solid, yield: 85%; HPLC purity: 99.90%. m. p. 255 °C (decomposed). ^{1}H NMR (300 MHz, DMSO-d_6) *δ (ppm)* 10.43 (s, 1H), 8.40 (d, J = 3.9 Hz, 2H), 7.97 (d, J = 7.6 Hz, 3H), 7.34 (d, J = 7.9 Hz, 2H), 6.89 (s, 1H), 6.24 (s, 1H), 2.38 (s, 6H). 13C NMR (75 MHz, DMSO-d_6) *δ (ppm)* 167.62, 166.03, 152.74, 151.09, 142.33, 140.61, 132.47, 132.12, 131.59, 129.41, 128.25, 119.95, 119.35, 118.78, 108.92, 108.03, 21.46, 13.89. MS (ESI-TOF) *m/z* calc'd for $C_{20}H_{17}NO_3S$ $[M+H]^+$ 352.1007, found 352.0998.

*4.1.3.11. 3-(4-Methylbenzamido)-5-(5-acetylthiophen-2-yl)benzoic acid (**11k**).* A white solid, yield: 85%; HPLC purity: 95.88%. m. p. 281 °C (decomposed) 1H NMR (300 MHz, DMSO-d_6) *δ* (ppm) 13.29 (s, 1H), 10.47 (s, 1H), 8.49 (d, J = 1.6 Hz, 2H), 8.00 (t, J = 1.6 Hz, 1H), 7.98 (d, J = 4.0 Hz, 1H), 7.94 (d, J = 8.2 Hz, 2H), 7.69 (d, J = 4.0 Hz, 1H), 7.37 (d, J = 8.1 Hz, 2H), 2.57 (s, 3H), 2.40 (s, 3H). 13C NMR (75 MHz, DMSO-d_6) *δ* (ppm) 191.15, 167.15, 166.13, 150.55, 143.71, 142.52, 140.92, 135.65, 133.76, 132.79, 131.91, 129.47, 128.23, 126.09, 121.75, 121.66, 26.88, 21.51. MS (ESI-TOF) *m/z* calc'd for C21H17N1O4S [M+H]+ 380.0957, found 380.0952.

*4.1.3.12. 3-(4-Methylbenzamido)-5-(furan-2-yl)benzoic acid (**11l**).* A white solid, yield: 81%; HPLC purity: 95.90%. m. p. 247 °C (decomposed). ^{1}H NMR (300 MHz, DMSO-d_6) *δ (ppm)* 13.16 (s, 1H), 10.38 (s, 1H), 8.21 (d, J = 10.8 Hz, 1H), 8.10 (t, J = 6.3 Hz, 2H), 7.98 (t, J = 5.3 Hz, 2H), 7.90 (d, J = 8.8 Hz, 1H), 7.80–7.70 (m, 1H), 7.33 (d, J = 7.9 Hz, 2H), 6.89 (d, J = 2.5 Hz, 1H), 2.38 (s, 3H). ^{13}C NMR (75 MHz, DMSO-d_6) *δ (ppm)* 167.78, 166.08, 144.89, 142.23, 140.54, 140.11, 133.12, 132.39, 132.15, 129.33, 128.20, 125.84, 122.00, 120.40, 121.95, 109.10, 21.35. MS (ESI-TOF) *m/z* calc'd for $C_{15}H_{19}NO_4$ $[M+H]^+$ 322.1079, found 322.1077.

*4.1.3.13. 3-(4-Methylbenzamido)-5-(furan-3-yl)benzoic acid (**11m**).* A white solid, yield: 87%; HPLC purity: 96.04%. m. p. 224 °C (decomposed). ^{1}H NMR (300 MHz, DMSO-d_6) *δ (ppm)* 10.38 (s, 1H), 8.25 (d, J = 16.0 Hz, 2H), 7.97 (q, J = 9.7, 6.8 Hz, 3H), 7.75 (s, 1H), 7.33 (d, J = 7.7 Hz, 2H), 6.85 (d, J = 3.2 Hz, 1H), 6.60 (t, J = 2.8 Hz, 1H), 2.38 (s, 3H). ^{13}C NMR (75 MHz, DMSO-d_6) *δ (ppm)* 167.39, 166.08, 142.82, 142.41, 140.76, 134.80, 132.55, 132.05, 129.44, 129.19, 128.24, 126.88, 124.76, 121.33, 121.26, 120.42, 21.50. MS (ESI-TOF) *m/z* calc'd for $C_{15}H_{19}NO_4$ $[M+H]^+$ 322.1079, found 322.1079.

*4.1.3.14. 3-(4-Methylbenzamido)-5-(5-methylfuran-2-yl)benzoic acid (**11n**).* A white solid, yield: 89%; HPLC purity: 98.89%. m. p. 286 °C (decomposed). ^{1}H NMR (300 MHz, DMSO-d_6) *δ (ppm)* 10.42 (s, 1H), 8.40 (s, 2H), 7.95 (d, J = 7.7 Hz, 3H), 7.33 (d, J = 7.9 Hz, 2H), 6.88 (s, 1H), 6.23 (s, 1H), 2.37 (s, 6H). ^{13}C NMR (75 MHz, DMSO-d_6) *δ (ppm)* 167.58, 166.00, 152.71, 151.06, 142.29, 140.57, 132.43, 132.08, 131.55, 129.37, 128.22, 119.92, 119.31, 118.75, 108.89, 108.00, 21.43, 13.86. MS (ESI-TOF) *m/z* calc'd for $C_{20}H_{17}NO_4$ $[M+H]^+$ 336.1236, found 336.1234.

*4.1.3.15. 3-(4-Methylbenzamido)-5-(3,4-dimethylisoxazol-5-yl)benzoic acid (**11o**).* A white solid, yield: 89%; HPLC purity: 97.84%. m. p. 219 °C (decomposed). ^{1}H NMR (400 MHz, DMSO-d_6) *δ (ppm)* 13.15 (s, 1H), 10.43 (s, 1H), 8.45 (t, J = 1.8 Hz, 1H), 8.05 (t, J = 1.9 Hz, 1H), 7.92 (d, J = 1.8 Hz, 1H), 7.90 (d, J = 1.9 Hz, 1H), 7.62 (t, J = 1.6 Hz, 1H), 7.37 (s, 1H), 7.35 (s, 1H), 2.46 (s, 3H), 2.40 (s, 3H), 2.27 (s, 3H). ^{13}C NMR (75 MHz, DMSO-d_6) *δ (ppm)* 167.49, 166.15, 165.98, 158.40, 142.37, 140.51, 132.37, 132.14, 130.97, 129.42, 128.26, 124.87, 124.74, 120.50, 115.73, 21.47, 11.86, 11.01.MS (ESI-TOF) *m/z* calc'd for $C_{20}H_{18}N_2O_4$ $[M+H]^+$ 351.1345., found 351.1340.

*4.1.3.16. 3-(4-Methylbenzamido)-5-(1H-pyrrol-2-yl)benzoic acid (**11p**).* A grey powder, yield: 74%; HPLC purity: 96.84%. m. p. 158–159 °C. ^{1}H NMR (300 MHz, DMSO-d_6) *δ (ppm)* 11.50 (s, 1H), 10.33 (s, 1H), 8.24 (d, J = 23.6 Hz, 2H), 8.00–7.89 (m, 3H), 7.36 (d,

J = 7.8 Hz, 2H), 6.87 (s, 1H), 6.50 (s, 1H), 6.16 (s, 1H), 2.40 (s, 3H). ^{13}C NMR (101 MHz, DMSO-d_6) δ *(ppm)* 167.81, 165.91, 142.27, 140.23, 134.13, 132.17, 130.79, 129.43, 129.17, 128.19, 120.49, 120.16, 119.80, 119.06, 109.75, 106.61, 21.50. MS (ESI-TOF) *m/z* calc'd for $C_{19}H_{16}N_2O_3$ $[M+H]^+$ 321.1239, found 321.1233.

*4.1.3.17. 3-(4-Methylbenzamido)-5-(1H-pyrazol-3-yl)benzoic acid (**11q**).* A pale yellow solid, yield: 81%; HPLC purity: 98.04%. m. p. 68 °C (decomposed) ^{1}H NMR (400 MHz, DMSO-d_6) δ *(ppm)* 10.48 (s, 1H), 8.41 (t, J = 1.7 Hz, 1H), 8.38 (t, J = 2.0 Hz, 1H), 7.91 (d, J = 7.9 Hz, 2H), 7.76 (t, J = 1.7 Hz, 1H), 7.67−7.58 (m, 2H), 7.35 (d, J = 7.9 Hz, 2H), 2.39 (s, 3H). ^{13}C NMR (75 MHz, DMSO-d_6) δ *(ppm)* 166.56, 166.27, 142.58, 141.45, 133.88, 133.42, 132.60, 131.99, 129.43, 129.29, 128.23, 126.94, 126.58, 121.88, 120.38, 21.46. MS (ESI-TOF) *m/z* calc'd for $C_{18}H_{15}N_3O_3$ $[M+Na]^+$ 322.1192, found 322.1188.

4.2. Biological evaluation

4.2.1. $P2Y_{14}R$ inhibitory activity screening

HEK293 cell lines stably expressing $P2Y_{14}R$ were plated in 384-well plates approximately 24h before assay at the density of 10 000 cells per well. Cells were incubated with 7.5 μL induction buffer containing Forskolin, UDPG and various concentrations of test compounds for 30 min at 37 °C. Then $P2Y_{14}R$ inhibitory activities were evaluated by detecting the levels of cAMP in HEK293 cell lysates with cAMP-Glo™ Assay Kits (Promega, WI, USA) followed the manufacturer's instructions and calculated IC_{50} values.

4.2.2. In vivo Murine gout model (MSU-induced inflammation) assay

ICR male mice were bred and housed in a conventional animal facility. All animals used for the experiments were between 8 and 12 weeks old. Mice were injected with monosodium urate (MSU) crystals (1.5 mg) suspended in 10 μL of phosphate-buffered saline (PBS, pH 7.4) to simulate acute gouty arthritis. Test compounds were administered by intravenous injection (25.6 μM/kg) into the footpads. The positive control, PPTN (10 μM), and **11m** (10 μM) was administered subcutaneously (sc), immediately after subcutaneous injection of MSU crystals on the paw plantar surface. PPTN and **11m** was dissolved in DMSO. Control mice received an equivalent volume of PBS (pH 7.4). After 24 h of MSU stimulation, foot tissues were extracted and stored for further analysis. As for the mice air pouch inflammation model, it was formed in the backs of ICR mice by subcutaneous injection of sterile air as previously described. On day 7, MSU crystals (2 mg suspended in 1 ml of PBS) and PPTN or **11m** were injected into the pouch. 24 h later, the air pouch lavages were collected and processed for pyroptosis assay.

4.2.3. Western blot

The mice foot tissues were lysed in a RIPA buffer, and the lysate was harvested by centrifugation at 12 000 rpm for 10 min. Aliquots of protein (40 μg/lane) were separated by 8−12% SDS-PAGE and transferred to polyvinylidene fluoride membranes (Millipore Corporation, Boston, MA, USA). Subsequently, the membranes were blocked for 2 h in 5% nonfat dry milk-TBS-0.1% Tween 20. 2 h later, the blots were incubated with primary antibodies at 4 °C overnight followed by a 2 h incubation with a horseradish peroxidase-conjugated secondary anti-rabbit antibody at room temperature. Finally, protein bands were visualized using enhanced chemiluminescence (ECL) detection solution (Beyotime, China) and scanned with a Chemiluminescence imaging system (Gel Catcher 2850, China).

4.2.4. Pyroptosis assay

Cell suspensions from the air pouch were centrifuged at 3000 rpm for 5 min. For the pyroptosis measurement, active Caspase-1 and PI fluorescence of samples were evaluated using flow cytometry. Active caspase-1 was measured by FLICA 660 Caspase-1 Detection Kit (Immunochemistry Technologies, U.S.A.) according to the manufacturer's instruction and propidium iodide (PI) was used to assess cells with membrane pores (Beyotime Biotechnology, Nanjing, CN).

4.2.5. Microsomal stability assay

Liver microsomal incubations were conducted in triplicate. Incubation mixtures consisted of 20 mM of each test compound, 0.2 mg/mL human liver microsomes, and 1 mM cofactor NADPH in a total volume of 400 mL of 100 mM potassium phosphate buffer (pH 7.4 containing 5 mM $MgCl_2$).The mixture was shaken for 5 min for preincubation in a shaking water bath at 37 °C. For metabolic stability studies, aliquots of 50 μL of the incubation sample mixture were collected at 0, 5, 10, 15, 30, and 45 min. After collection of samples, the reaction was terminated with 100 μL of EtOAc containing the internal standard. The mixture was then centrifuged at 10000g to remove the protein and the supernatant was subsequently applied to LC-MS/MS analysis. The natural log of the amount of parent compound remaining was plotted against time to calculate the rate of disappearance and the half-life of the tested compounds.

4.2.6. Statistical analysis

Statistical analysis was performed using an Unpaired Student t-test, or one-way ANOVA, in GraphPad Prism version 8 (GraphPad software Inc., CA, USA). Alpha value was 0.05 and the confidence interval was 95%. Data are presented as the means ± standard deviation (SD) of at least three independent experiments, and was considered statistically significant when $p < 0.05$.

4.3. Water solubility

The compound powder and PBS buffer (pH 7.4) were mixed in Eppendorf tubes, followed by vigorously vortexed for 1 min and sonicated for another 10 min at room temperature, then the mixture was incubated with shaking overnight to ensure compound saturation at room temperature. Compound suspensions were centrifuged at 10 000 RPM for 15 min, and supernatants were filtered through 0.22 mm syringe filters. Concentrations of compound in the supernatants were determined by UV-3000 absorption spectrometry with standard curves and absorption extinction coefficient in the same buffer pre-determined.

Declaration of competing interest

The authors declare that they have no known competing financial interests or personal relationships that could have appeared to influence the work reported in this paper.

Acknowledgements

This work has been financially supported by National Natural Science Foundation of China (No. 82073685, 81773745 and 81872867), "Double First-Class" University project (CPU2018GF02), Open-end Funds of Jiangsu Key Laboratory of Marine Pharmaceutical Compound Screening (HY201902) and the "Qinglan Project" of Jiangsu Province.

Appendix A. Supplementary data

Supplementary data to this article can be found online at https://doi.org/10.1016/j.ejmech.2021.113313.

References

[1] G. Burnstock, Purinergic signalling: therapeutic developments, Front. Pharmacol. 8 (2017) 661.
[2] G. Burnstock, Purine and pyrimidine receptors, Cell. Mol. Life Sci. 64 (12) (2007) 1471–1483.
[3] B. Geoffrey, Introduction: P2 receptors, Curr. Top. Med. Chem. 4 (8) (2004) 793–803.
[4] M. Rafehi, C.E. Muller, Tools and drugs for uracil nucleotide-activated P2Y receptors, Pharmacol. Ther. 190 (2018) 24–80.
[5] E.R. Lazarowski, T.K. Harden, UDP-Sugars as extracellular signaling molecules: cellular and physiologic consequences of P2Y14 receptor activation, Mol. Pharmacol. 88 (2015) 151–160.
[6] J.K. Chambers, L.E. Macdonald, H.M. Sarau, R.S. Ames, K. Freeman, et al., A G protein-coupled receptor for UDP-glucose, J. Biol. Chem. 275 (2000) 10767–10771.
[7] M.O. Barrett, J.I. Sesma, C.B. Ball, P.S. Jayasekara, K.A. Jacobson, et al., A selective high-affinity antagonist of the P2Y14 receptor inhibits UDP-glucose-stimulated chemotaxis of human neutrophils, Mol. Pharmacol. 84 (1) (2013) 41–49.
[8] M. Kinoshita, K. Nasu-Tada, K. Fujishita, K. Sato, S. Koizumi, Secretion of matrix metalloproteinase-9 from astrocytes by inhibition of tonic P2Y(14)-receptor-mediated signal(s), Cell. Mol. Neurobiol. 33 (1) (2013) 47–58.
[9] Z.G. Gao, Y. Ding, K.A. Jacobson, UDP-glucose acting at P2Y14 receptors is a mediator of mast cell degranulation, Biochem. Pharmacol. 79 (6) (2010) 873–879.
[10] R.T. Amison, S. Arnold, B.G. O'Shaughnessy, S.J. Cleary, J. Ofoedu, M. Idzko, et al., Lipopolysaccharide (LPS) induced pulmonary neutrophil recruitment and platelet activation is mediated via the P2Y1 and P2Y14 receptors in mice, Pulm. Pharmacol. Therapeut. 45 (2017) 62–68.
[11] J.I. Sesma, C.D. Weitzer, A. Livraghi-Butrico, H. Dang, S. Donaldson, N.E. Alexis, et al., UDP-glucose promotes neutrophil recruitment in the lung, Purinergic Signal. 12 (4) (2016) 627–635.
[12] J. Meister, D. Le Duc, A. Ricken, R. Burkhardt, J. Thiery, H. Pfannkuche, et al., The G protein-coupled receptor P2Y14 influences insulin release and smooth muscle function in mice, J. Biol. Chem. 289 (34) (2014) 23353–23366.
[13] J. Xu, H. Morinaga, D. Oh, P. Li, A. Chen, S. Talukdar, et al., GPR105 ablation prevents inflammation and improves insulin sensitivity in mice with diet-induced obesity, J. Immunol. 189 (4) (2012) 1992–1999.
[14] A. Azroyan, V. Cortez-Retamozo, R. Bouley, R. Liberman, Y.C. Ruan, E. Kiselev, et al., Renal intercalated cells sense and mediate inflammation via the P2Y14 receptor, PloS One 10 (3) (2015), e0121419.
[15] D.J. Moore, P.R. Murdock, J.M. Watson, R.L.M. Faull, H.J. Waldvogel, P.G. Szekeres, et al., GPR105, a novel Gi/o-coupled UDP-glucose receptor expressed on brain glia and peripheral immune cells, is regulated by immunologic challenge: possible role in neuroimmune function, Mol. Brain Res. 118 (1–2) (2003) 10–23.
[16] C. Cekic, J. Linden, Purinergic regulation of the immune system, Nat. Rev. Immunol. 16 (3) (2016) 177–192.
[17] H. Uratsuji, Y. Tada, C.S. Hau, S. Shibata, M. Kamata, T. Kawashima, et al., Monosodium urate crystals induce functional expression of P2Y14 receptor in human keratinocytes, J. Invest. Dermatol. 136 (6) (2016) 1293–1296.
[18] M.A. Battistone, A.C. Mendelsohn, R.G. Spallanzani, A.S. Allegretti, R.N. Libermanl, et al., Pro-inflammatory P2Y14 receptor inhibition protects against ischemic acute kidney injury in mice, J. Clin. Invest. 130 (7) (2020) 3734–3749.
[19] H. Li, W. Jiang, S. Ye, M. Zhou, C. Liu, et al., P2Y(14) receptor has a critical role in acute gouty arthritis by regulating pyroptosis of macrophages, Cell Death Dis. 11 (5) (2020) 394–408.
[20] R. Lu, Z. Zhang, C. Jiang, Recent progress on the discovery of P2Y14 receptor antagonists, Eur. J. Med. Chem. 175 (2019) 34–39.
[21] D. Guay, C. Beaulieu, M. Belley, S.N. Crane, J. DeLuca, Y. Gareau, et al., Synthesis and SAR of pyrimidine-based, non-nucleotide P2Y14 receptor antagonists, Bioorg. Med. Chem. Lett 21 (10) (2011) 2832–2835.
[22] J.Y. Gauthier, M. Belley, D. Deschenes, J.F. Fournier, S. Gagne, Y. Gareau, et al., The identification of 4,7-disubstituted naphthoic acid derivatives as UDP-competitive antagonists of P2Y14, Bioorg. Med. Chem. Lett 21 (10) (2011) 2836–2839.
[23] J. Robichaud, J.F. Fournier, S. Gagne, J.Y. Gauthier, M. Hamel, Y. Han, et al., Applying the pro-drug approach to afford highly bioavailable antagonists of P2Y(14), Bioorg. Med. Chem. Lett 21 (14) (2011) 4366–4368.
[24] Y.H. Jung, J. Yu, Z. Wen, S. Veronica, P.K. Tadeusz, B.P. Ngan, et al., Exploration of alternative scaffolds for P2Y14 receptor antagonists containing a biaryl core, J. Med. Chem. 63 (17) (2020) 9563–9589.
[25] E. Kiselev, M.O. Barrett, V. Katritch, S. Paoletta, C.D. Weitzer, K.A. Brown, et al., Exploring a 2-naphthoic acid template for the structure-based design of P2Y14 receptor antagonist molecular probes, ACS Chem. Biol. 9 (12) (2014) 2833–2842.
[26] A. Junker, R. Balasubramanian, A. Ciancetta, E. Uliassi, E. Kiselev, C. Martiriggiano, et al., Structure-based design of 3-(4-aryl-1H-1,2,3-triazol-1-yl)-Biphenyl derivatives as P2Y14 receptor antagonists, J. Med. Chem. 59 (13) (2016) 6149–6168.
[27] J. Yu, A. Ciancetta, S. Dudas, S. Duca, J. Lottermoser, K.A. Jacobson, Structure-guided modification of heterocyclic antagonists of the P2Y14 receptor, J. Med. Chem. 61 (11) (2018) 4860–4882.
[28] M. Zhou, S. Li, Song, Q. Hu, W. Liu, 4-(2-(4-chlorophenyl)-1- ((4-chlorophenyl) amino)ethyl)benzene-1,3-diol is a potential agent for gout therapy as a dual inhibitor of XOD and NLRP3, Phytomedicine 42 (2018) 9–17.
[29] Z. Zhang, K. Hao, H. Li, R. Lu, C. Liu, et al., Design, synthesis and anti-inflammatory evaluation of 3-amide-benzoic acid derivatives as novel P2Y14 receptor antagonists, Eur. J. Med. Chem. 181 (2019) 111564.